



Charging analysis and characterizations of COOH group functionalized graphene combined with paraffin wax as phase change material for thermal energy storage applications

Sumit Nagar¹ · Kamal Sharma¹ · Mahendra Singh¹ · Pramod Kumar¹ · A. K. Pandey²

Received: 3 November 2021 / Accepted: 6 April 2022 / Published online: 2 May 2022
© Akadémiai Kiadó, Budapest, Hungary 2022

Abstract

In this work to increase the thermal capacity and performance of pristine paraffin wax (phase change material), it is mixed with COOH group functionalized graphene. The various concentrations of graphene mixed with paraffin wax are 0.25 volume percent to 1 volume percent at an increment of 0.25 volume% at three different volumetric flow rates of 6.25 mL s⁻¹, 12.5 mL s⁻¹, and 25 mL s⁻¹. The charging performance is analyzed, and Fourier transform infrared spectroscopy (FTIR), X ray diffraction (XRD), differential scanning calorimetric (DSC) analysis, Thermo gravimetric analysis (TGA), field effective scanning electron microscopy, with energy dispersive spectroscopy are done for characterizing chemical structure, crystal structure, enthalpy, thermal stability, and microstructure, along with elemental composition, respectively. The results indicated that with increasing percentages of COOH group functionalized graphene the charging time decreases by 6.25–25% for the HTF flow rate 6.25 mL s⁻¹, 6.67–26.67% for HTF flow rate 12.5 mL s⁻¹, and 15.38–38% for HTF flow rate 25 mL s⁻¹ over pure paraffin wax owing to increasing percentage and thermal conductivity of COOH group functionalized graphene in paraffin wax. This advanced material with the help of XRD and FTIR also showed that the functionalized COOH graphene was chemically inert and did not lead to any new product being formed. Through TGA the advanced functional materials manifested that they were thermally very stable and by DSC it showed that it was having very high enthalpy of melting.

Keywords COOH group · Functionalized graphene · Paraffin wax · Characterization · Charging

Introduction

At low and high temperatures the temporary storage of thermal [1] energy in a body is called thermal energy storage system (TESS). The concept of TESS has made its presence felt since centuries. It was used by researchers, engineers, and scientists since past many years. Energy storage [2] plays an important role in energy conservation by reducing time and decrementing the rate mismatch between energy demand and supply. This leads to increased performance of energy systems by increment in systems reliability and

smoothing supply. Although sun provides, safe, clean, and an abundant source of energy, the supply of this energy is periodic following diurnal and yearly cycles; it is irregular often diffused and unpredictable. Its density is less compared with energy flux density found in conventional fossil energy devices like oil fired furnaces and coal based thermal power plants. Therefore, the requirement of storage of solar energy is very much necessary and the usage of solar energy presently poses trouble primarily because of inefficient storage and collection. The most significant characteristics of storage systems is the duration of time during which energy can be kept stored with some amount of acceptable losses. Due to the heat energy losses of heat transfer mechanisms like conduction, convection [3], and radiation the actual thermal energy storage may last for very short time. Another important point of a storage system is the energy capacity per unit volume. Therefore, good storage system should have small volume per unit of energy stored and long storage time.

In any required temperature range a large number of phase change materials (eutectic, inorganic, organic) are

✉ Sumit Nagar
sumit12_ab@rediffmail.com

¹ Department of Mechanical Engineering, GLA University, Mathura, Uttar Pradesh 281406, India

² Research Center for Nanomaterials and Energy Technology (RCNMET) Level 3, School of Engineering and Technology, Sunway University, 47500 Subang Jaya, Selangor Darul Ehsan, Malaysia

accessible. A phase change material (PCM) can be defined as a substance which has got high heat of fusion and is competent of melting and solidifying at a certain temperature range due to which it can store or release large amount of energy. The classification of thermal energy storage (TES) and PCM with their different types is shown in Fig. 1.

The present work is focused on charging analysis of paraffin wax (PCM) with COOH group functionalized graphene for thermal energy storage system and their characterizations. Some relevant literature reviews are mentioned below:

Gasia et al. [5] studied thermal behavior of paraffin wax as PCM for household hot water applications and industrial waste heat recovery. A complete thermal (laboratory) characterization was done like differential scanning calorimeter, thermo gravimetric analysis, thermo cycling and infrared spectroscopy. Nair et al. [6] used experimental study of PCM for thermal energy storage. To remove the mismatch between supply and demand of energy thermal energy storage plays a pivotal role. Thermal energy storage systems play a very important role in energy conservation. Kanimozhi et al. [7] studied thermal characteristics of charging and discharging [8] process using phase change materials. A storage tank was fabricated for enhancing the heat transfer rate from solar tank to PCM storage tank. This storage tank was used to

store large amount of energy. Performance evaluations of charging and discharging of experimental results was discussed in her work. Zhao et al. [9] by in situ polymerization prepared paraffin@graphene/melamine–formaldehyde microPCMs. The graphene [10] was used as Pickering stabilizer in their work. The morphology of the microPCMs were studied by SEM and DSC was used to evaluate thermal properties of the microPCMs. The outcome of their work was that the microPCMs possess significant application in the field of thermal energy storage applications. Liu et al. [11] enhanced the thermal properties of paraffin wax in TES by mixing it with exfoliated graphite sheets and graphene having mass fractions 0–2%. They performed various characterization like FTIR, DSC, TGA, SEM, and thermal conductivity test and finally concluded that the paraffin's thermal conductivity increased with mass% increase in graphene and exfoliated graphite sheet and the mixture was morphologically sound without any micro cracks although graphene and exfoliated graphite sheet mixed with paraffin wax remained chemically inert with each other. Kumar et al. [12] performed experimental work on paraffin wax mixed with COOH functionalized graphene at a volumetric flow rate of 12.5 mL s^{-1} of heat transfer fluid [13] (HTF) and deduced that charging time decreases with increasing

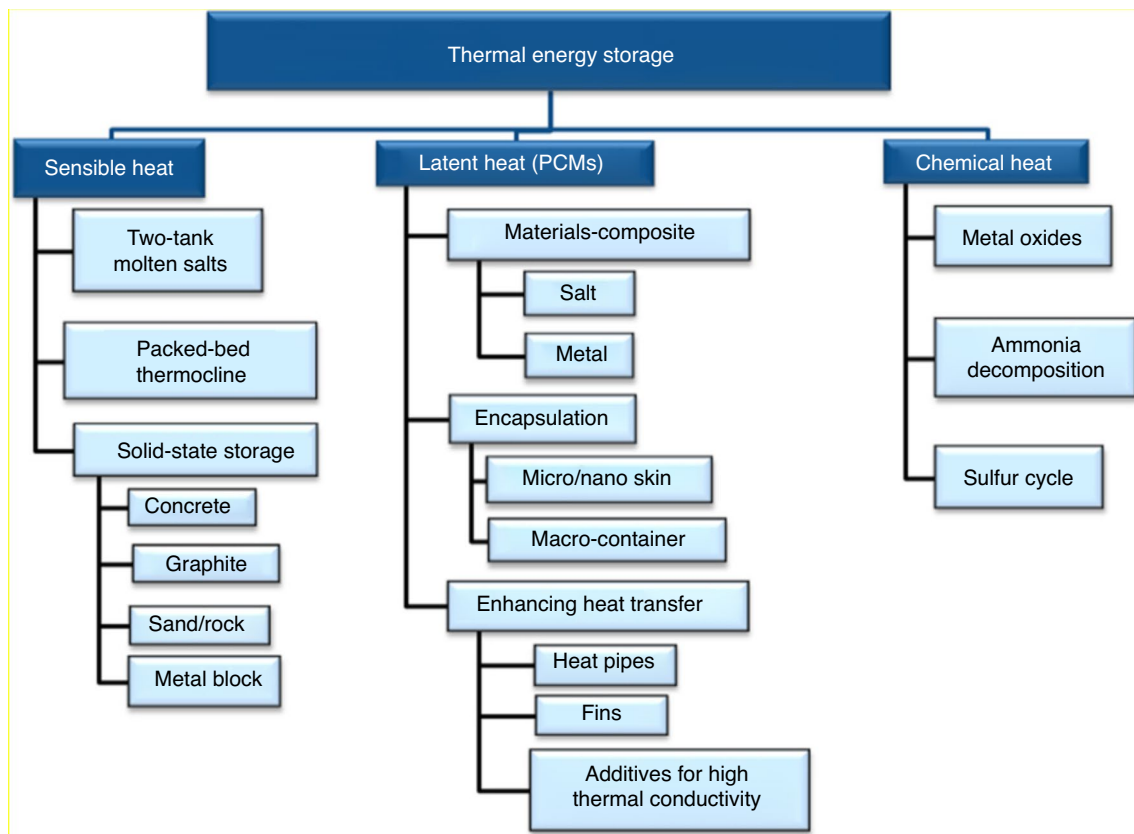


Fig. 1 Classification of PCM [4]

percentages of COOH functionalized graphene in paraffin wax by almost 30–50% at various volume% from 0.25 to 1% of COOH functionalized graphene. Singh et al. [14] used the same apparatus like Kumar et al. of TES and at a volumetric flow rate of 6.25 mL s^{-1} proved that the Charging time decreased by 30–50% of COOH functionalized graphene mixed with paraffin wax at various volume% from 0.25 to 1% of COOH functionalized graphene in paraffin wax.

There are many works where paraffin wax is doped with graphene and its derivative like graphene oxide [15], pristine graphene mixtures [9, 16], and exfoliated graphene sheets [11] but functionalized graphene (COOH group) mixed with Paraffin wax phase change materials (PCM) provided improved structural properties, enhanced thermal properties, prevents agglomeration and increases dispersibility in organic solvents. The charging time reduction is also achieved owing to increased thermal conductivity of the above-stated advanced functional materials. The main area of application involved in this work is the usage of paraffin wax (PCM) mixed with COOH functionalized graphene as battery. These materials can store energy and energy can be dissipated at the time of need. For example, in domestic hot water usage in cold countries. For the increment of heat storage and heat transfer rate PCMs are used in heat exchangers. The PCMs also reduce heat exchanger size and pipe line size. In buildings and residential areas in different countries for the purpose of air conditioning.

In this work the charging analysis and characterizations of pristine paraffin wax and paraffin wax mixed with nano [17, 18] additives (COOH group functionalized graphene) was done. The characterization techniques especially thermal characterization (DSC, TGA) showed that paraffin wax and paraffin wax mixed with COOH group functionalized graphene had very high latent heat of fusion per unit mass and high thermal stability. The charging time reduced with increasing% of COOH group functionalized graphene in paraffin wax and this observation tells us that the materials used in this work were having quality thermal storage properties. This research article connects chemical and crystal structure, micro structure and morphology, enthalpy of melting, and thermal stability with the reduction in charging times of Paraffin wax with nano additives. According to the authors this is the first time where characterization of COOH group functionalized graphene was done along with evaluation of PCMs energy storage capabilities for thermal energy storage applications.



Fig. 2 Before melting and stirring operation the basic PCM

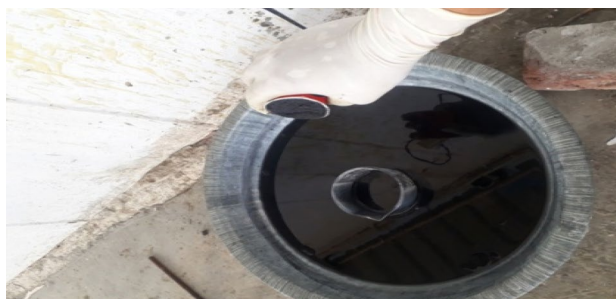


Fig. 3 After melting and stirring operation the composite PCM

Characterizations and experimental work

Materials and preparation of phase change composite

Properties like high heat storage capacity and high heat of fusion is present in paraffin wax which was procured from *Ecosense Sustainable Solutions Private limited*, India. Carboxyl (COOH) group functionalized graphene was purchased from *platonic nanotech private limited Jharkhand India*, which was used in doping paraffin wax (PCM). The Carboxyl (COOH) group based graphene nanoparticles in various volume percentage 0.25%, 0.5%, 0.75%, and 1% are mixed/doped with PCM paraffin wax. Firstly the paraffin wax is melted with the help of electric heaters till the PCM melts completely and when the PCM is warm and completely liquefied then the nano material is added and mixed/stirred resulting in a PCM composite as shown in Figs. 2 and 3.

Characterizations

Structure and morphology

Fourier transform infrared spectroscopy, FTIR with diamond ATR and Pellet accessories (PerkinElmer spectrum 2) was used in experimental spectra range $4000\text{--}400\text{ cm}^{-1}$ and sample to KBr ratio 1:99. Powdered XRD (Bruker D8 advance) was done in the range $10^{\circ}\text{--}80^{\circ}$ with scanning step 0.05° and scanning rate $1.2^{\circ}\text{ min}^{-1}$ for knowing the crystalloid phase. The standard operating condition for the XRD apparatus was voltage 40 mV and current 40 mA. The morphology and microstructure were observed from field emissions scanning electron microscope coupled with energy dispersive spectroscopy (EDS) detector Au Sputter Coater (FE-SEM: JEOL JSM -7610F plus EDS: OXFORD EDS LN2 free, AuCoater: JEOL Smart Coater).

Thermal properties

The temperatures like phase change temperature, enthalpy of melting, onset temperature, and ending temperature were calculated by DSC (PerkinElmer DSC 6000) having alumina crucible in heating range $5\text{--}90^{\circ}\text{ C}$ with heating rate of $10^{\circ}\text{ C min}^{-1}$ under nitrogen atmosphere. The thermo gravimetric analysis (PerkinElmer TGA 4000) was done from heating range $30\text{--}600^{\circ}\text{ C}$ at a heating rate of $10^{\circ}\text{ C min}^{-1}$ under nitrogen atmosphere. The thermal conductivity and thermal diffusivity was checked through LFA-447 apparatus by laser flash method.

Experimental set up and working

The actual photograph and schematic diagram of TESS is as shown in Figs. 4 and 5, respectively. Firstly the water is filled in cold Heat transfer fluid (HTF) tank. Then the water is supplied from the cold HTF tank by pump to HTF tank at the top of the machine. Whenever there is a condition of over flow the pump is made to close and to supply warm water to the heat exchangers the electric heater is turned on. When the water becomes sufficiently warm by the help of appropriate valves the water flows through the heat exchanger. The hot water dissipates the heat by convection and conduction when flowing through the heat exchanger and the



Fig. 4 Photograph of thermal energy storage system (TESS)

thermocouples are mounted on different cylinders to give knowledge about the temperature like PCM inlet and PCM outlet temperature which is used in various calculations as shown in the subsequent section.

Calculation with formulas

Analysis of heat exchanger

Heat transfer for the HTF per unit length of cylinder can be expressed as,

$$q = \frac{T_{av,HTF,chg,j} - T_{amb}}{R}, \quad (1)$$

$T_{av,HTF,chg,j}$, average temperature of HTF during charging $^{\circ}\text{C}$; T_{amb} , ambient temperature $^{\circ}\text{C}$; R , total thermal resistance of the PCM cylinder through which HTF flows; h_i , convective (inner) heat transfer coefficient; h_o , convective (outer) heat transfer coefficient.

The calculation of h_o for turbulent flow [19] depends upon Prandtl and Grashof's number whose value depends upon the type of flow, laminar or turbulent,

$$R = \frac{1}{h_i A_i} + \frac{\ln(r_2/r_1)}{2\pi k_1 L_1} + \frac{\ln(r_3/r_2)}{2\pi k_2 L_2} + \frac{\ln(r_4/r_3)}{2\pi k_3 L_3} + \frac{\ln(r_5/r_4)}{2\pi k_4 L_4} + \frac{\ln(r_6/r_5)}{2\pi k_5 L_5} + \frac{1}{h_o A_o}. \quad (2)$$

solid PCM melts by absorbing heat from the HTF which is water to complete the charging process. The used HTF gets collected in the used HTF tank, and the HTF flows continuously till the PCM is fully charged and melted. The various

Calculation of h_i

Following is the basic equation to calculate h_i ,

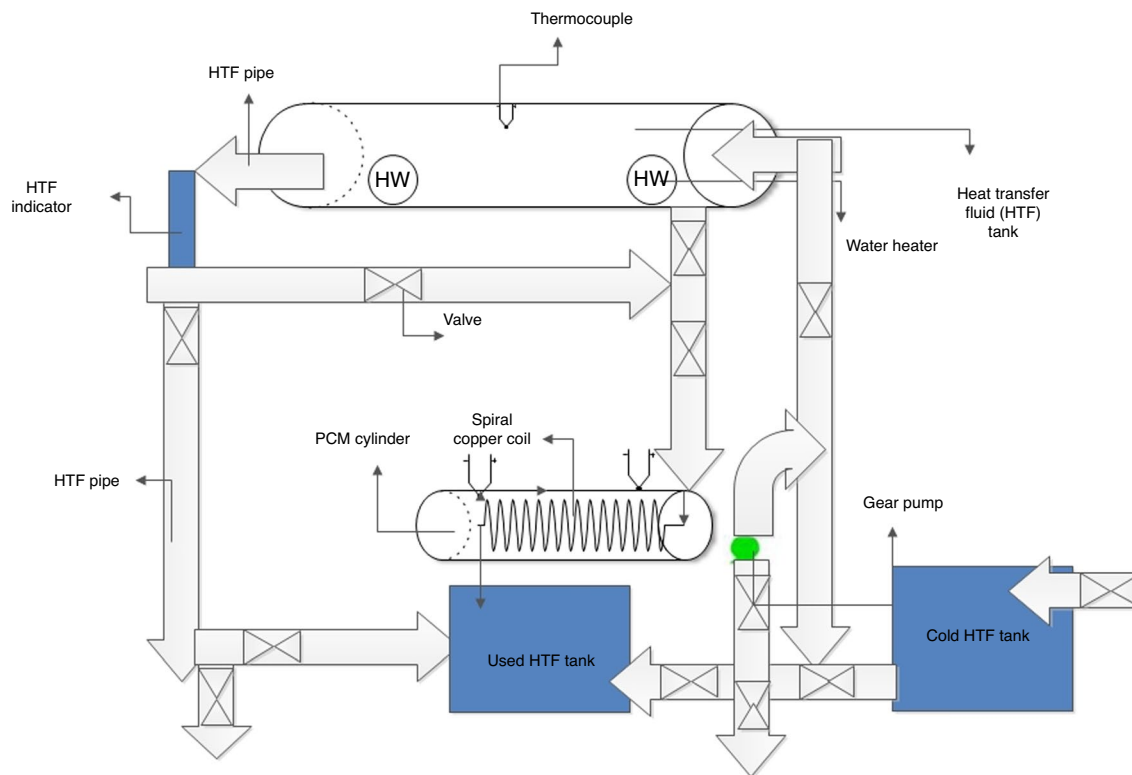


Fig. 5 Schematic diagram of TESS [12]

$$h_i = \frac{N_u K_w}{D_i}, \tag{3}$$

where the Nusselt number N_u can be calculated by using the following empirical formula.

(a) Laminar flow and constant heat supply for smooth circular tube,

$$N_u = \frac{h_i D_i}{k_w} = 4.36, \tag{4}$$

where k_w , thermal conductivity of water; D_i , internal diameter of copper tube.

(b) Laminar flow and constant surface temperature for smooth circular tube,

$$N_u = \frac{h_i D_i}{k_w} = 3.66, \tag{5}$$

(c) For fully-completed turbulent flow

$$N_u = 0.023 Re^{0.8} Pr^n,$$

where n has the value equal to 0.4 for heating and value 0.3 for cooling in the fluid flowing through the tube,

$$Re = \frac{D_i V}{\nu},$$

$$V = \frac{m_w}{\rho_w A_i},$$

where V velocity of water through copper pipe [20–22]; m_w , mass flow rate of water; ν , kinematic viscosity; Re , Reynolds number; ρ_w is the density of water.

The h_o can be calculated from Grashof number and Prandtl number under turbulent flow with its elementary equations.

Charging period calculations

In this stage the hot HTF flows through the heat exchanger and give energy to PCM.

Here, energy input during charging,

Table 1 Cylinder specification [4]

Parameters	Copper tube		PCM		SS pipe		Insulation		GI cover		Unit
Internal radius	r_1	0.00545	r_2	0.00635	r_3	0.07	r_4	0.072	r_5	0.122	m
Outer radius	r_2	0.00635	r_3	0.07	r_4	0.072	r_5	0.122	r_6	0.1229	m
Conductivity	k_1	390	k_2	0.22	k_3	16	k_4	0.033	k_5	16	$\text{W m}^{-1} \text{K}^{-1}$
Length	L_1	6.25	L_2	0.9	L_3	0.9	L_4	0.9	L_5	0.9	m
Heat transferring surface cross-sectional area	A_i	9.3305×10^{-5}							A_o	0.2139×10^{-5}	m^2

Table 2 Heat exchanger dimension [4]

S. No.	Parameters	Value	Unit
1	Inner diameter of heat exchanger shell	140	mm
2	Heat exchanger shell length	900	mm
3	Heat exchanger shell thickness	2	mm
4	Inner diameter of heat exchanger tube (Cu)	11.5	mm
5	Heat exchanger tube (HET) outer diameter (Cu)	12.7	mm
6	Thickness of HET (Cu)	0.6	mm
7	Length of HET (Cu)	9000	mm
8	Heat exchanger spiral count	33	
9	HET pipe conductivity	300	$\text{W m}^{-1} \text{K}^{-1}$

$$E_{\text{in,chg}} = \dot{m}_{\text{HTF}} C_{\text{HTF}} (T_{\text{i,HTF,chg}} - T_{\text{amb}}) \times \text{time}_{\text{chg}}, \quad (6)$$

Energy accumulated during charging,

$$E_{\text{acc,chg}} = E_{\text{in,chg}} - \{E_{\text{losses,chg(i+ii)}}\}, \quad (7)$$

Energy loss during charging,

$$E_{\text{loss,chg,i}} = q \times L_{\text{ins}} \times \text{time}_{\text{chg}}, \quad (8)$$

Other energy losses, energy loss without absorption,

$$E_{\text{loss,chg,ii}} = \dot{m}_{\text{HTF}} C_{\text{HTF}} (T_{\text{o,HTF,chg}} - T_{\text{amb}}) \times \text{time}_{\text{chg}}, \quad (9)$$

$$\text{Charging efficiency} = E_{\text{acc,chg}} / E_{\text{in,chg}}. \quad (10)$$

$E_{\text{in,chg}}$, the input energy during charging period; $E_{\text{acc,chg}}$, the energy accumulated during charging; $E_{\text{loss,chg,i}}$, the environmental losses; $E_{\text{loss,chg,ii}}$, the energy loss without absorption; \dot{m}_{HTF} , the mass flow rate of HTF; C_{HTF} , the specific heat capacity of water; $T_{\text{i,HTF,chg}}$, the HTF inlet temperature during charging; T_{amb} , the ambient temperature; time_{chg} , the charging time; $T_{\text{o,HTF,chg}}$, the HTF outlet temperature during charging; L_{ins} , the length of insulation; q , the Rate of heat transfer for HTF per unit length (W m^{-1}).

The cylinder specification and heat exchanger dimensions used for calculations are as mentioned in Tables 1 and 2.

The cylinder with heat exchanger is as shown in Fig. 6. In between the copper tube of heat exchanger and cylinder cover (stainless steel) PCM is kept, and then, it is surrounded

**Fig. 6** Cylinder and heat exchanger [12]

by insulation or foam and GI cover to prepare the PCM cylinder.

Results and discussions

The result of charging analysis [23] and structural characterization as well as thermal characterization [24] is dealt with in this section.

Table 3 Time required for charging at flow rate 6.25 mL s^{-1}

PCM	Time required (in min) for charging the cylinder at flow rate 6.25 mL s^{-1}
Paraffin wax (PW)	160
COOH functionalized graphene (0.25%) in PW	150
COOH functionalized graphene (0.5%) in PW	140
COOH functionalized graphene (0.75%) in PW	130
COOH functionalized graphene (1%) in PW	120

Table 4 Time required for charging at flow rate 12.5 mL s^{-1}

PCM	Time required (in min) for charging the cylinder at flow rate 12.5 mL s^{-1}
Paraffin wax (PW)	150
COOH functionalized graphene (0.25%) in PW	140
COOH functionalized graphene (0.5%) in PW	130
COOH functionalized graphene (0.75%) in PW	120
COOH functionalized graphene (1%) in PW	110

Table 5 Time required for charging at flow rate 25 mL s^{-1}

PCM	Time required (in min) for charging the cylinder at flow rate 25 mL s^{-1}
Paraffin wax (PW)	130
COOH functionalized graphene (0.25%) in PW	110
COOH functionalized graphene (0.5%) in PW	100
COOH functionalized graphene (0.75%) in PW	90
COOH functionalized graphene (1%) in PW	80

Charging rate analysis

It can be observed from the experiments that pristine paraffin wax takes the most time in case of charging and as the concentration of COOH group functionalized graphene increases in paraffin wax the charging time decreases. This phenomenon is explained with the help of Tables 3, 4, and 5. It can be inferred from the table that increasing volume concentration of nano additives and increase in flow rate of heat transfer fluid (HTF) are able to charge the cylinder very quickly. In case of a battery [25, 26] where all need faster charging such systems with PCMs combined with nano additives can be used. The PCMs can store energy during phase change and dissipate whenever it is required.

The charging rate can be described in forms of temperature ($^{\circ}\text{C}$) per unit time (minutes). The charging process of paraffin wax is shown in Fig. 7a, b which measures the PCM inlet and PCM outlet temperature, respectively versus time in minutes. It was observed that higher flow rate and increase in the concentration of graphene reduced the cylinder charging time as discussed above. The reason of this is high thermal conductivity of graphene which is due

to covalent sp^2 bonding between carbon atoms in the nano COOH group functionalized graphene mixed with paraffin wax. Figures 8a, b, 9a, b, 10a, b, and 11a, b depicts the change in PCM inlet and outlet temperature with respect to time for 0.25%, 0.5%, 0.75%, and 1% COOH graphene mixed with paraffin wax, respectively. The relevant and important point in these graphs are the constant, and steady increase in temperature with respect to time till the PCMs melting point which is in the range of $55\text{--}57$ ($^{\circ}\text{C}$) is reached, and the cylinder is completely charged.

Input energy and accumulated energy analysis

The input energy increases with increase in flow rate of the heat transfer fluid (HTF) which is water due to heat transfer phenomenon. Moreover, the input energy remains nearly constant for a particular flow rate as shown in Figs. 12–16 for pure paraffin wax, 0.25% COOH group functionalized graphene [27] mixed with paraffin wax, 0.50% COOH group functionalized graphene mixed with paraffin wax, 0.75% COOH group functionalized graphene mixed with paraffin wax, and 1% COOH group functionalized graphene mixed

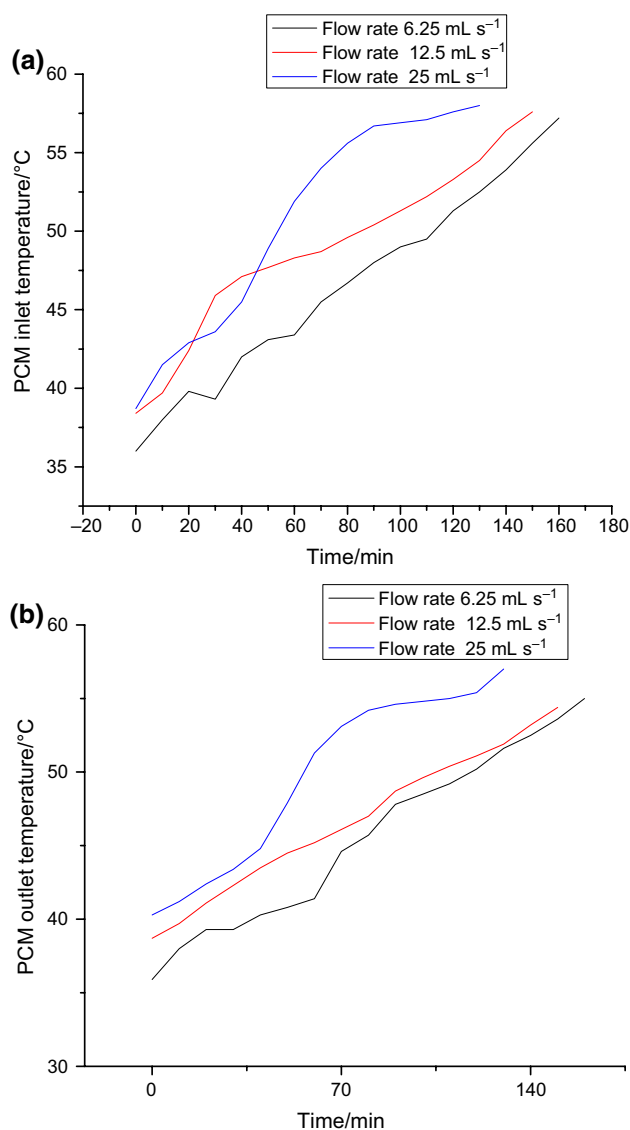


Fig. 7 **a** PCM inlet temperature with respect to time at different flow rates for pristine Paraffin wax. **b** PCM outlet temperature with respect to time at different flow rates for pristine Paraffin wax

with paraffin wax, respectively. This high amount of energy has two kinds of losses energy loss during charging (piping losses) and energy loss without absorption. The energy loss without absorption depends upon the doped PCMs energy absorbing capacity. When these two losses are subtracted from input energy then the energy accumulated during charging is obtained which is a critical factor in determining the charging efficiencies. The curve for accumulated energy as shown in Figs. 17–21 for pure paraffin wax, 0.25% COOH group functionalized graphene mixed with paraffin wax, 0.50% COOH group functionalized graphene mixed with paraffin wax, 0.75% COOH group functionalized graphene mixed with paraffin wax, and 1% COOH group functionalized graphene mixed with paraffin wax, respectively. The

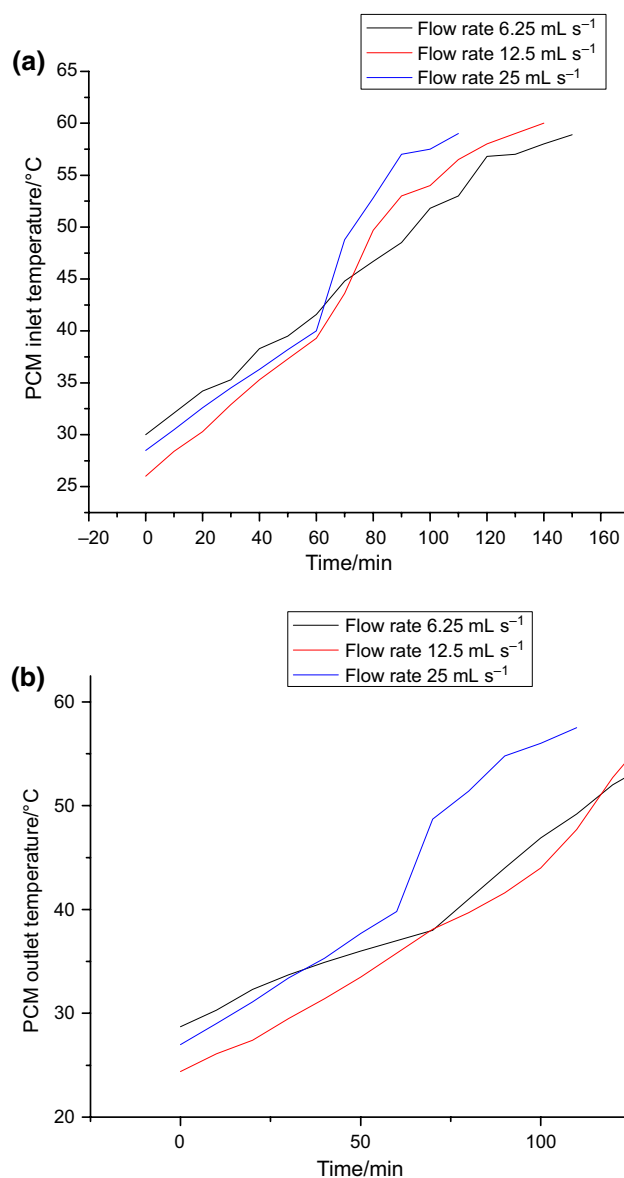


Fig. 8 **a** PCM inlet temperature with respect to time at different flow rates for paraffin wax mixed with 0.25 volume percent COOH functionalized graphene. **b** PCM Outlet temperature with respect to time at different flow rates for paraffin wax mixed with 0.25 volume percent COOH functionalized graphene

curves of accumulated energy have zigzag shape because as the flow of HTF depends upon the HTF stored in HTF tank at the top cylinder of capacity 50 L, more water is to be pumped up to maintain the continuous flow of the HTF storage tank from the cold water storage tank at the bottom of machine of capacity 120 L. The cold water mixes with hot water inside the HTF tank thereby decreasing the temperature along with accumulated energies, and the graph shows downward trend. After electrical heating as the temperature and energy rises of the HTF in HTF tank the graph shows an upward trend and this clarifies all the graphs zigzag shape

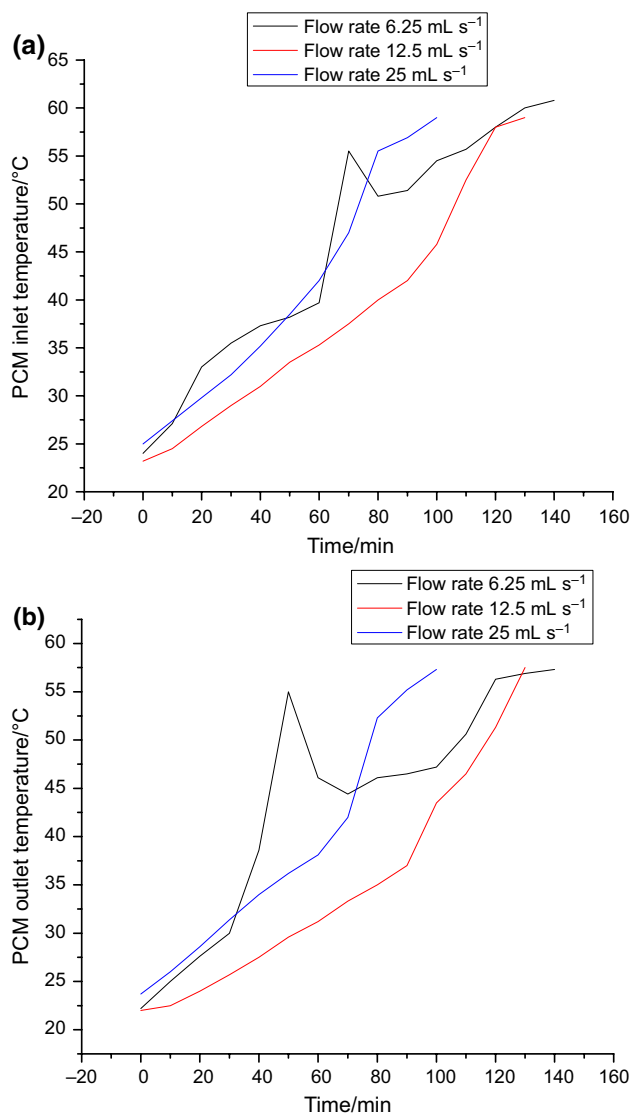


Fig. 9 **a** PCM inlet temperature with respect to time at different flow rates for paraffin wax mixed with 0.5 volume percent COOH functionalized graphene. **b** PCM Outlet temperature with respect to time at different flow rates for paraffin wax mixed with 0.5 volume percent COOH functionalized graphene

for accumulated energies. The input energy and accumulated energy are functions of HTF inlet and outlet temperatures.

Fourier transform infrared spectroscopy (FTIR)

The chemical compatibility and identification of chemical compounds was done by FTIR for various percentages of COOH functionalized graphene based paraffin waxes. Figure 22 demonstrates the FTIR spectrum for pristine paraffin wax and various percentages (0.25–1 volume%) of COOH functionalized graphene in paraffin wax. The characteristic transmittance band showed peaks at 2916 cm⁻¹,

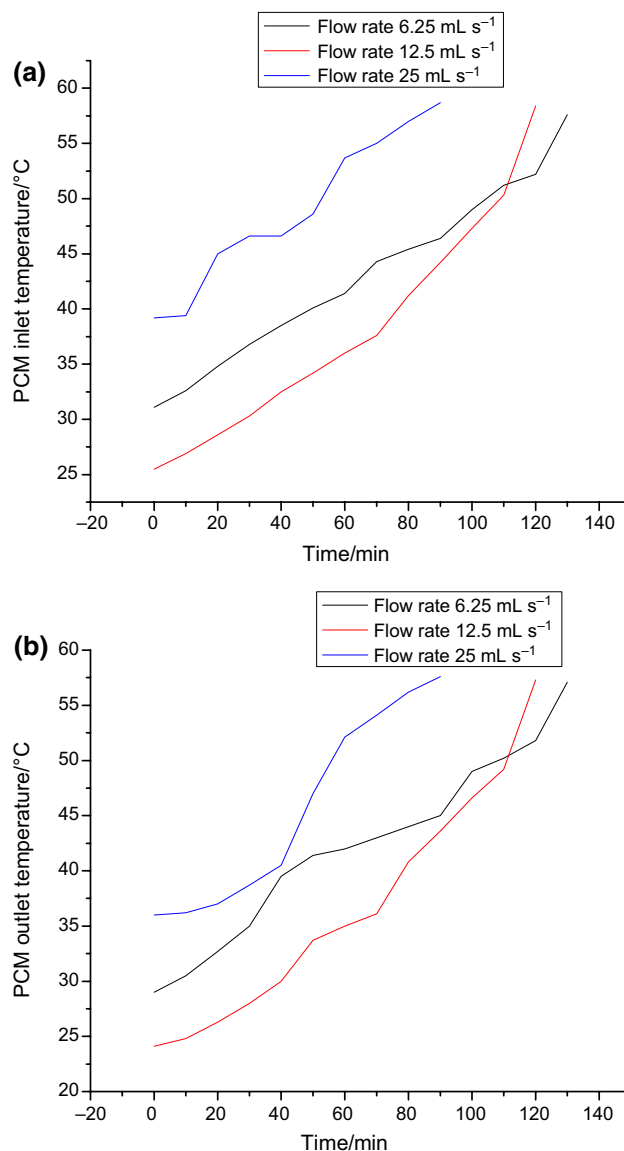


Fig. 10 **a** PCM inlet temperature with respect to time at different flow rates for paraffin wax mixed with 0.75 volume percent COOH functionalized graphene. **b** PCM Outlet temperature with respect to time at different flow rates for paraffin wax mixed with 0.75 volume percent COOH functionalized graphene

2848 cm⁻¹, 1463 cm⁻¹, 1376 cm⁻¹, and 723 cm⁻¹. The band at 2916 cm⁻¹ was due to asymmetric stretching vibration of CH₃ group, the band at 2848 cm⁻¹ was due to symmetric stretching vibration of CH₂ group, the bands at 1463 cm⁻¹ and 1376 proves that the carboxylic group is present in the mixture along with O–H group bending and the graphene is COOH group functionalized graphene. The peak at 723 cm⁻¹ was due to rocking vibration of CH₂ in the fingerprint region. The transmittance bands of pristine graphene and functionalized graphene was very weak as compared to paraffin wax. These results also paved the way for the

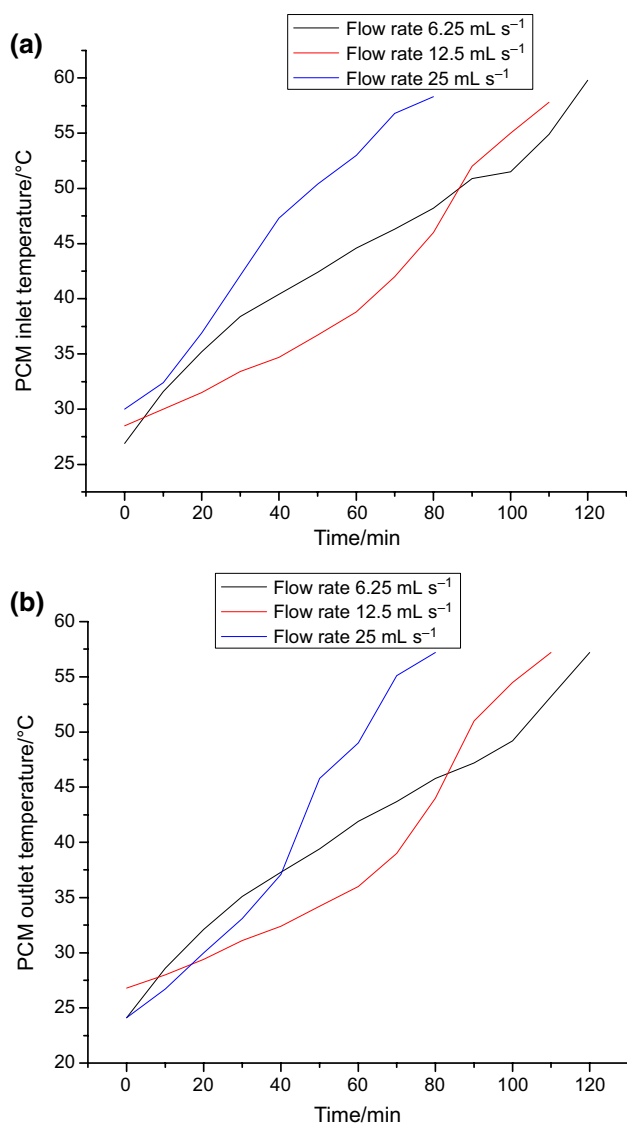


Fig. 11 **a** PCM inlet temperature with respect to time at different flow rates for paraffin wax mixed with 1 volume percent COOH functionalized graphene. **b** PCM Outlet temperature with respect to time at different flow rates for paraffin wax mixed with 1 volume percent COOH functionalized graphene

observation that paraffin wax and COOH group functionalized graphene were chemically inert and the chemical reaction was minimal.

X-ray diffraction (XRD)

Figure 23 reveals the XRD patterns of pristine paraffin wax and paraffin wax mixed with various volume percent (0.25, 0.5, 0.75, and 1) of COOH group functionalized graphene. There are two diffraction peaks observed for pristine paraffin wax at $2\theta = 21.31^\circ$ and 23.68° which is characteristic of paraffin wax having diffraction of crystal planes (0 1 2) and (1

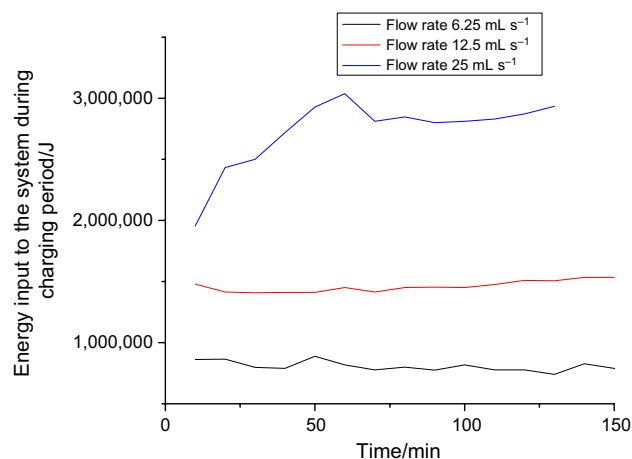


Fig. 12 Energy input to the system during charging versus time for pristine paraffin wax

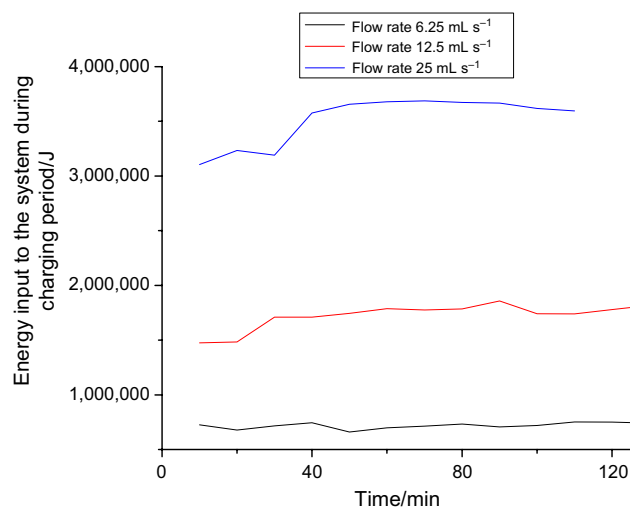


Fig. 13 Energy input to the system during charging versus time for 0.25 volume percent COOH functionalized graphene mixed with PW

1 0), respectively. 0.25 volume percent COOH group functionalized graphene mixed with paraffin wax shows peaks at $2\theta = 21.50^\circ$ and 23.86° having diffraction of crystal planes (2 0 0) and (2 1 0) along with many other peaks with very little intensity like peaks at $2\theta = 17.63^\circ$, 19.10° , and 36.09° . Similarly, 0.5 volume percent COOH group functionalized graphene has peaks at $2\theta = 21.39^\circ$ and 23.77° with many other low intensity peaks like $2\theta = 14.86^\circ$, 16.16° , 40.36° , and 40.57° . 0.75 volume percent COOH group functionalized graphene mixed with paraffin wax has peaks at $2\theta = 21.50^\circ$ and 23.87° having diffraction of crystal planes (2 0 0) and (0 2 0), respectively, and due to the addition of COOH group functionalized graphene it shows low intensity peaks at 16.24° , 18° , 19.63° , 39.88° , and 40.51° . 1 volume percent COOH functionalized graphene shows peaks at $2\theta = 21.47^\circ$

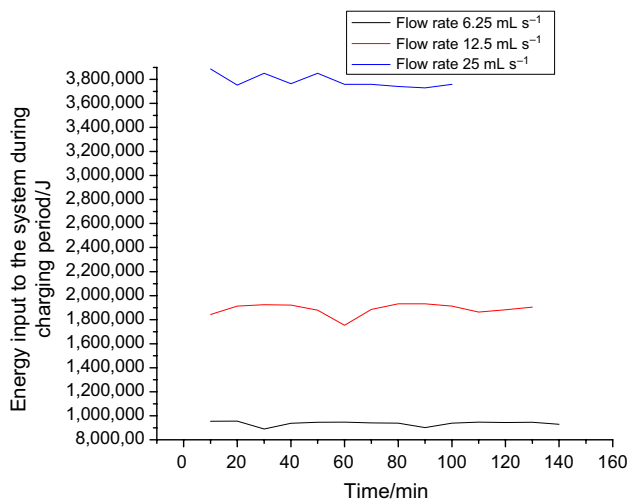


Fig. 14 Energy input to the system during charging versus time for 0.5 volume percent COOH functionalized graphene mixed with PW

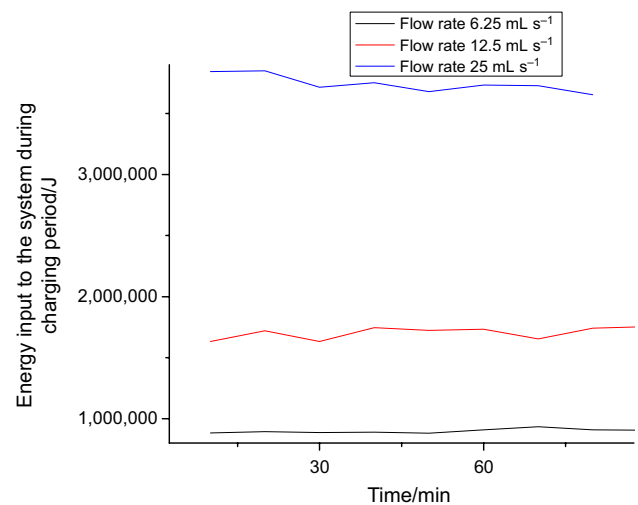


Fig. 16 Energy input to the system during charging versus time for 1 volume percent COOH functionalized graphene mixed with PW

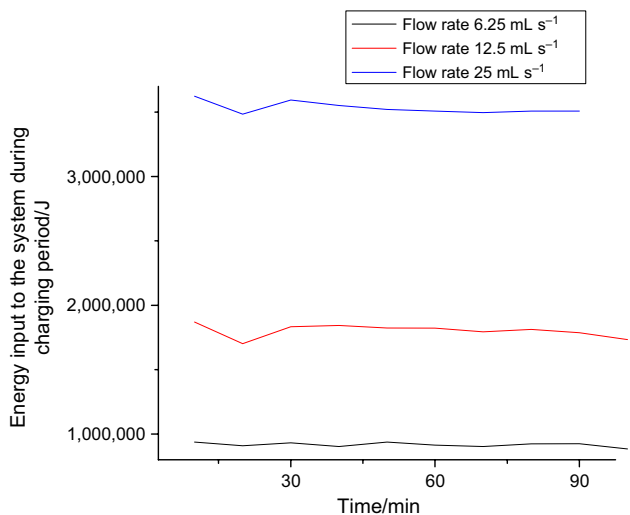


Fig. 15 Energy input to the system during charging versus time for 0.75 volume percent COOH functionalized graphene mixed with PW

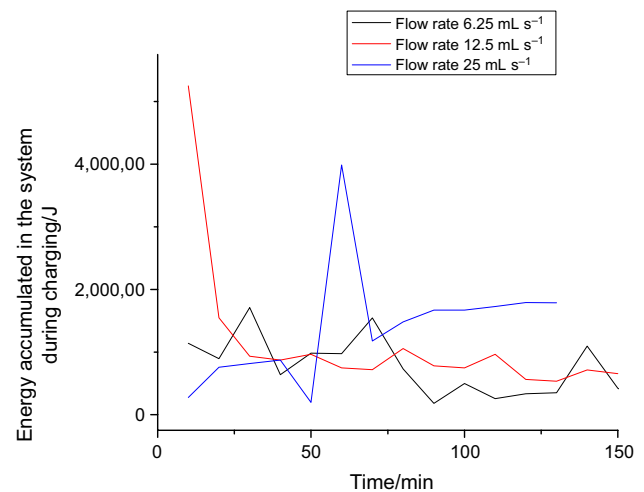


Fig. 17 Energy accumulated in the system during charging versus time for pristine paraffin wax

and 23.85° due to diffraction of crystal planes (1 2 1) and (2 0 2) along with many low intensity diffraction peaks at $2\theta = 14.47^\circ, 15.20^\circ, 36.03^\circ,$ and 40.45° .

The XRD pattern clearly indicates that there is no chemical reaction between COOH group functionalized graphene and paraffin wax and due to high content of paraffin wax its characteristic peaks shows little deviation from the pristine paraffin wax peaks and crystal planes.

Differential scanning calorimetry (DSC)

Figure 24 presents the melting curve of paraffin wax along with different volume percent of COOH functionalized

graphene in paraffin wax. As this paper covers charging aspects, the endothermic and melting description is sufficient for this analysis. The onset (T_{onset}), peak (T_{peak}), ending (T_{ending}) temperatures, and enthalpy of melting (H_m) are as shown in Table 6. Paraffin wax has favorable heat storage density and plays a major role in storing heat. The endothermic peak temperature shows a solid–liquid phase transition peak at around 61°C for all the samples. The enthalpy of melting also increases with increase in COOH functionalized graphene concentration and is nearly equal for 0.75 volume% functionalized graphene and 1 volume% functionalized graphene.

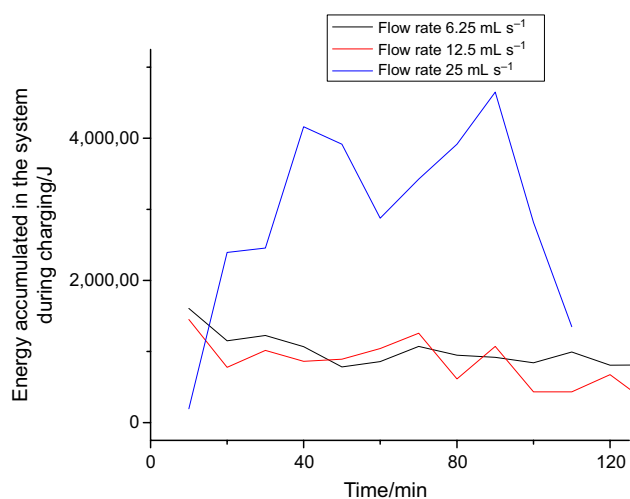


Fig. 18 Energy accumulated in the system during charging versus time for 0.25 volume percent COOH functionalized graphene mixed with PW

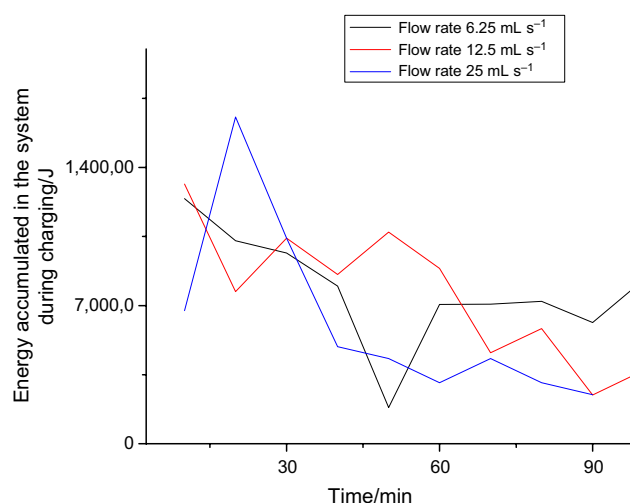


Fig. 20 Energy accumulated in the system during charging versus time for 0.75 volume percent COOH functionalized graphene mixed with PW

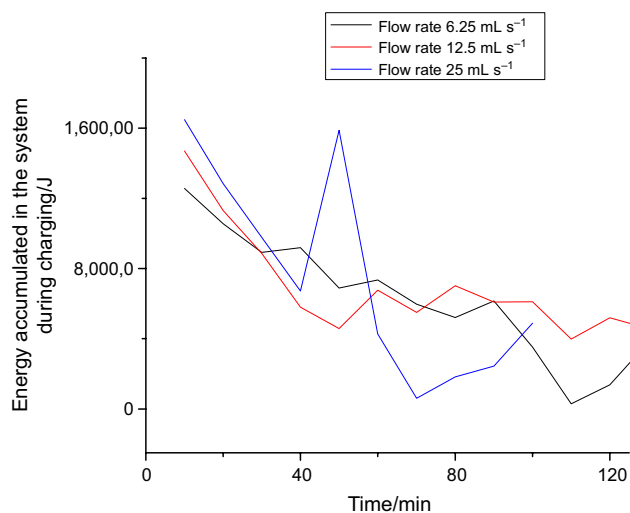


Fig. 19 Energy accumulated from the system during charging versus time for 0.5 volume percent COOH functionalized graphene mixed with PW

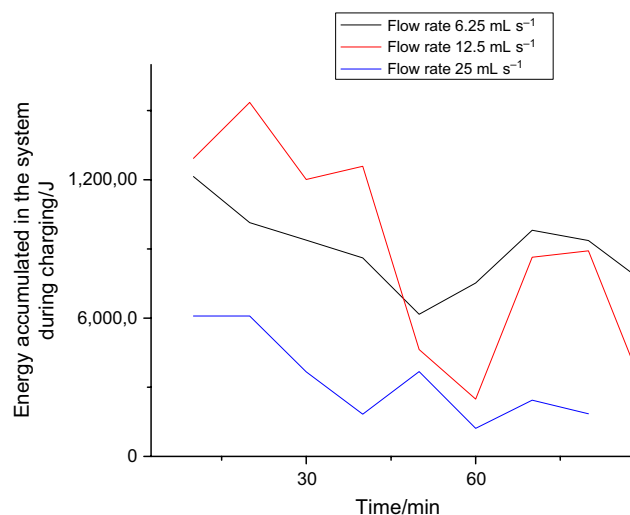


Fig. 21 Energy accumulated in the system during charging versus time for 1 volume percent COOH functionalized graphene mixed with PW

Thermo gravimetric analysis (TGA)

Thermo gravimetric analysis was done for finding if the samples are thermally stable or not as presented in Fig. 25. The overall tendency of mass loss of composite was found out to be consistent with that of the pristine paraffin wax. The mass of the samples begin to drop when the temperature reached 200 °C.

The mass loss was maximum in the region of 250–410 °C. Due to thermal decomposition of sample the mass loss was very slow after 410 °C. This curve also indicated that the graphene has little influence on thermal inertia of paraffin

wax. The mass loss is higher for various functionalized graphene paraffin wax samples than that of pristine paraffin wax. The graph trend depicted that the all the five samples were thermally stable and can be used as thermal energy storage materials for various applications.

Field emission scanning electron microscopy (FESEM)

Figure 26 shows the FESEM images or the morphology of pristine paraffin wax and paraffin wax with different concentrations of COOH functionalized graphene. The

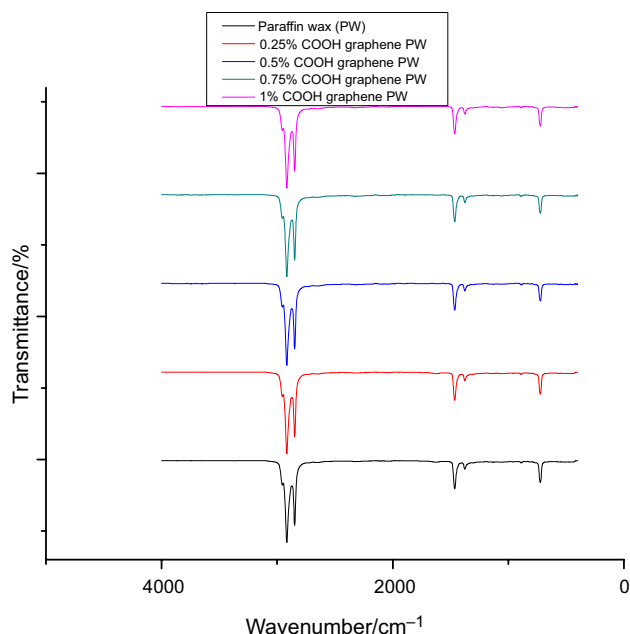


Fig. 22 FTIR details of Paraffin wax and 0.25 volume% to 1% COOH group functionalized graphene mixed with paraffin wax (PW)

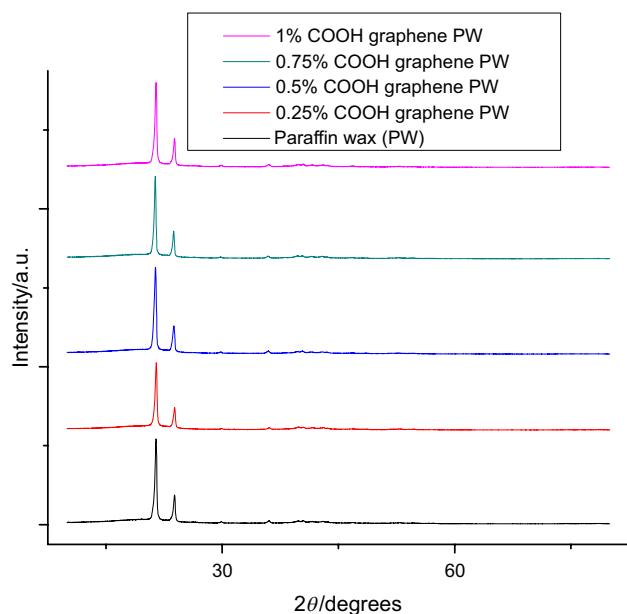


Fig. 23 XRD details of Paraffin wax and 0.25 volume% to 1% COOH group functionalized graphene mixed with paraffin wax (PW)

microstructure of paraffin wax is as depicted in Fig. 26a, and there appears no micro cracks and loose surfaces. The layers of paraffin wax looks crumpled in structure. The 0.25 volume percentages of COOH functionalized graphene mixed with paraffin wax are also shown in Fig. 26b along with measurement of particle size. The various nano-particles

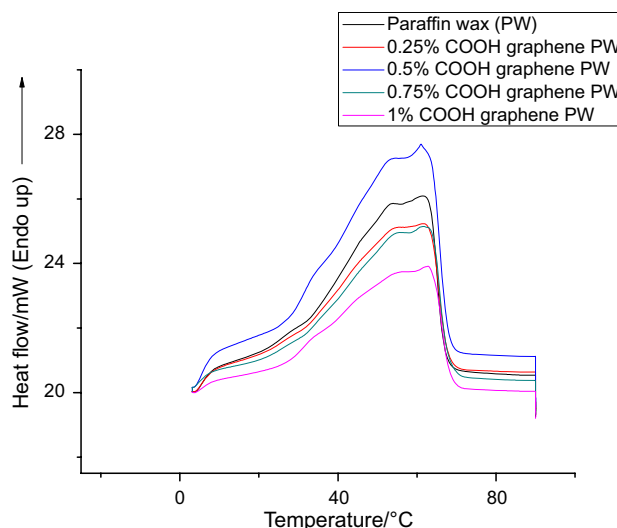


Fig. 24 DSC details of Paraffin wax and 0.25 volume% to 1% COOH group functionalized graphene mixed with paraffin wax (PW)

(COOH functionalized graphene) comes in contact with paraffin wax and their respective sizes are as small as $4.62 \mu\text{m}$. The other FESEM photographs are presented in Fig. 26c–e of 0.5, 0.75, and 1 volume% COOH graphene mixed with paraffin wax. The surface no longer appears to be smooth for these (0.5, 0.75, 1%) concentrations due to the addition of nano particle. They also constructed the framework for enhancing heat transfer and the nanoparticle were properly mixed with paraffin wax.

Energy dispersive spectroscopy (EDS)

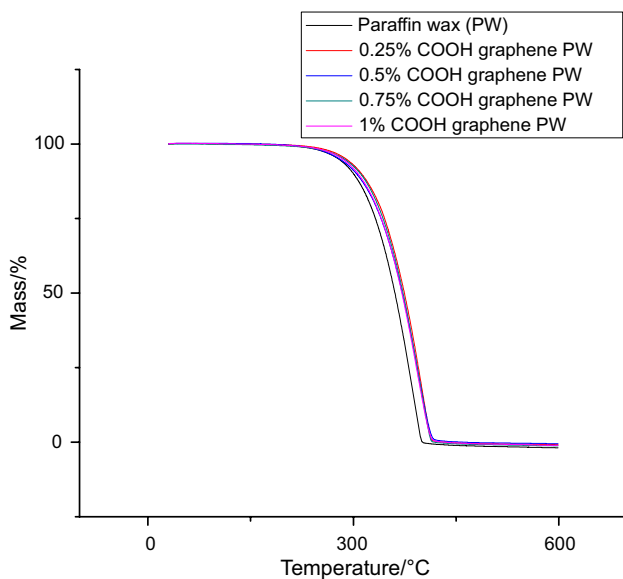
The elemental analysis is done by EDS, and the chemical composition is checked as atomic percentage and mass percentage level. The various elemental composition is shown in Tables 7–11 for paraffin wax and different volume percentage of COOH functionalized graphene mixed with paraffin wax along with the characteristic graphs in Fig. 27a–e. The other component present is hydrogen, but it is not shown due to limitation of EDS analysis as the hydrogen has not got K shell or it can be better understood as the only electron is shared with k shell in covalent bonding.

Thermal conductivity tests

The thermal conductivity and thermal diffusivity was also checked as shown in Fig. 28. It was observed that with increasing volume percentages of graphene in the mixture the thermal conductivity increases along with thermal diffusivity for functionalized graphene mixed with paraffin wax owing to very high thermal conductivity of pristine COOH functionalized Graphene. There was an increment of 7.6%, 10.8%, 29.8%, and 43.4% for COOH functionalized

Table 6 DSC Enthalpy and temperature details

Sample	Onset temperature/ $^{\circ}\text{C}$	Peak temperature/ $^{\circ}\text{C}$	Ending temperature/ $^{\circ}\text{C}$	Enthalpy of melting $H_m/\text{J g}^{-1}$
Paraffin wax	27.70	61.57	66.84	153.05
COOH functionalized graphene (0.25%)	25.85	61.75	67.69	154.77
COOH functionalized graphene (0.5%)	24.31	61.03	67.79	162.26
COOH functionalized graphene (0.75%)	26.66	61.75	67.65	167.98
COOH functionalized graphene (1%)	23.79	62.94	68.23	167.43

**Fig. 25** TGA details of Paraffin wax and 0.25 volume% to 1% COOH group functionalized graphene mixed with Paraffin wax

graphene mixed with paraffin wax having graphene volume concentrations 0.25%, 0.5%, 0.75%, and 1%, respectively, over pristine paraffin wax whose thermal conductivity was 0.184 W m K^{-1} . The thermal diffusivity too showed increase in values by 1.73%, 11.30%, 30.43%, and 43.48% for COOH functionalized graphene mixed with paraffin wax having graphene volume concentrations 0.25%, 0.5%, 0.75%, and 1%, respectively, over pristine paraffin wax whose thermal diffusivity was $0.115 \text{ mm}^2 \text{ s}^{-1}$. Thermal diffusivity tells us how fast the heat diffuses through the specimen.

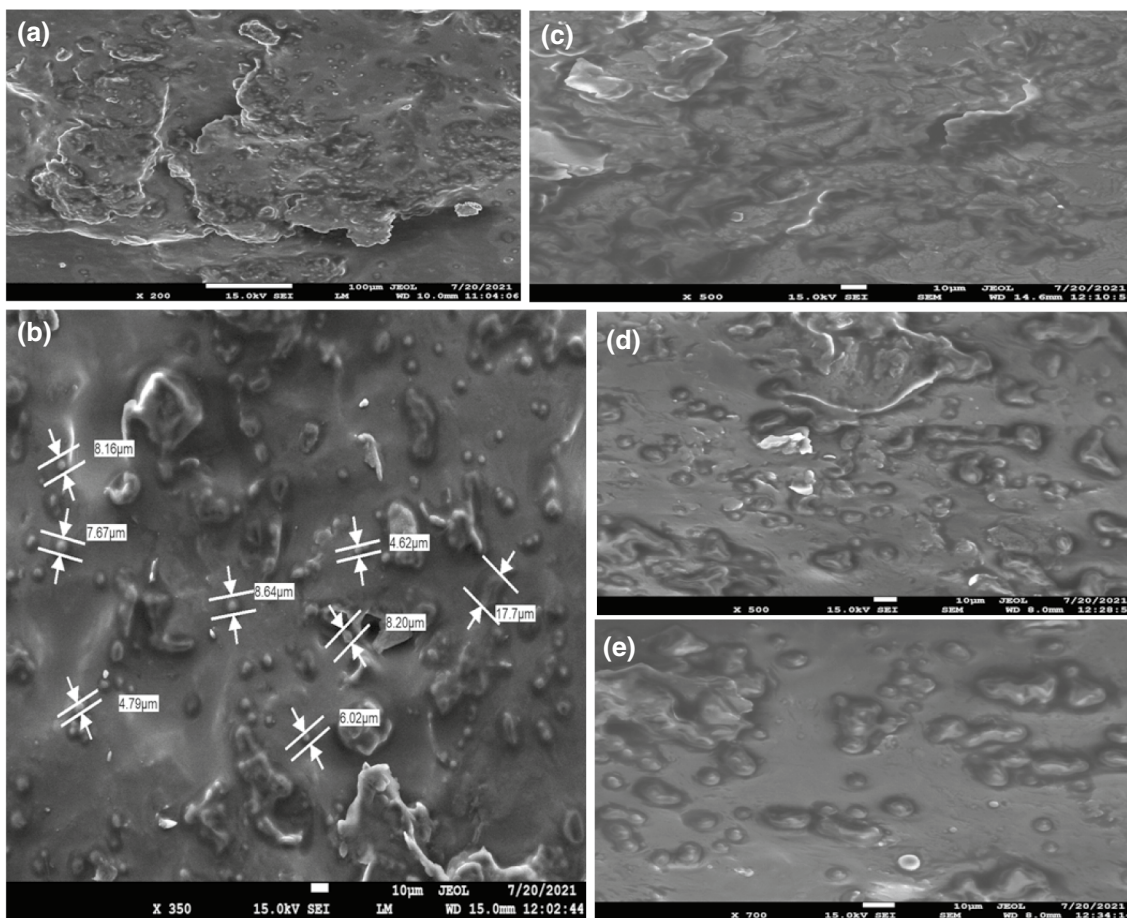


Fig. 26 FESEM images of **a** paraffin wax, **b** 0.25 volume% COOH group graphene mixed with PW, **c** 0.5 volume% COOH group graphene mixed with PW. **d** 0.75 volume% COOH group graphene mixed with PW. **e** 1 volume% COOH group graphene mixed with PW

Table 7 Atomic and mass% of pure PW

Element	Mass/%	Atom/%
C	74.47	79.53
O	25.53	20.47

Table 8 Atomic and mass% of 0.25 volume% COOH group graphene mixed with PW

Element	Mass/%	Atom/%
C	97.23	96.35
O	2.77	3.65

Table 9 Atomic and mass% of 0.50 volume% COOH group graphene mixed with PW

Element	Mass/%	Atom/%
C	93.45	95
O	6.55	5

Table 10 Atomic and mass% of 0.75 volume% COOH group graphene mixed with PW

Element	Mass/%	Atom/%
C	93.31	94.90
O	6.69	5.10

Table 11 Atomic and mass% of 1 volume% COOH group graphene mixed with PW

Element	Mass/%	Atom/%
C	96.35	95.19
O	3.65	4.81

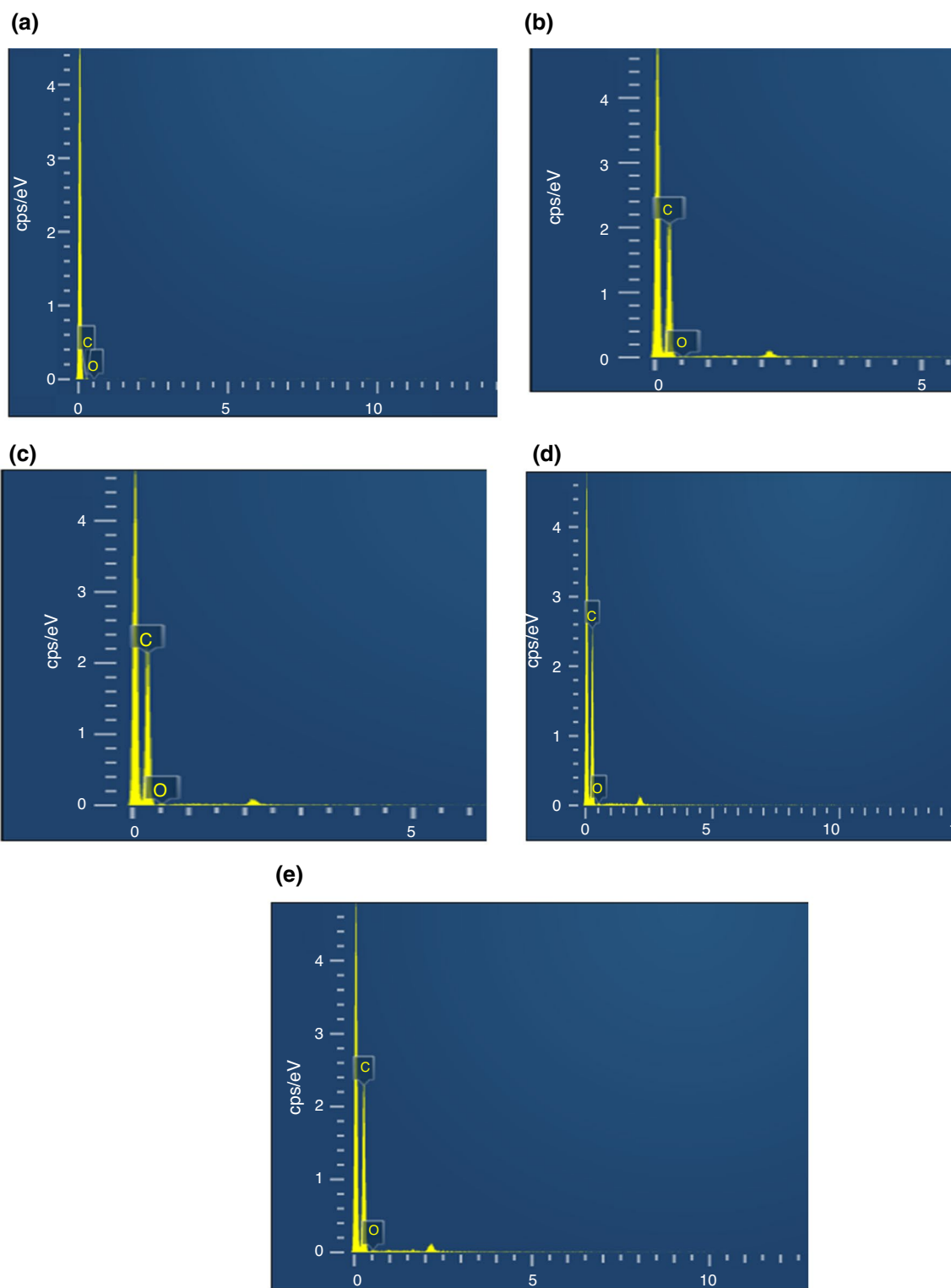


Fig. 27 EDS analysis images of **a** paraffin wax, **b** 0.25 volume% COOH group graphene mixed with PW, **c** 0.5 volume% COOH group graphene mixed with PW. **d** 0.75 volume% COOH group graphene mixed with PW. **e** 1 volume% COOH group graphene mixed with PW

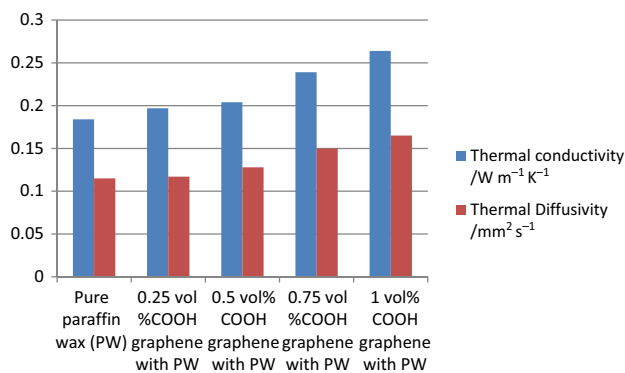


Fig. 28 Thermal conductivities and thermal diffusivities of various samples considered

Conclusions

Some important conclusions can be derived from the above-mentioned experiments

1. The charging time decreases and faster charging of the cylinder is done when the concentration of COOH group functionalized graphene increases in the PCM (paraffin wax) also
2. Increase in flow rate of the HTF leads to faster charging of the PCM cylinder. The input and accumulated energies can also be found out which leads to calculation of charging efficiencies.
3. The chemical compatibility and chemical structure was identified by FTIR, and this experiment showed the presence of COOH group in the chemical structure of graphene. XRD showed peaks that were characteristic of paraffin wax and the little content of COOH graphene did not show the presence of any new chemical structure due to chemical reaction between COOH graphene and paraffin wax. The FTIR and XRD curves proved the fact that there was no chemical reaction between COOH graphene and paraffin wax and COOH functionalized graphene remained chemically inert. The FESEM analysis manifested that there were no micro cracks and loose surfaces present in the surface of the COOH functionalized graphene although the structure was a bit crumpled and the size of graphene attached to the COOH functionalized graphene particle was as small as 4.62 μm due to the mixture of nano-powdered graphene with paraffin wax. The EDS analysis also proved the fact that Carbon and oxygen with their above-mentioned mass and atomic percent were present in the mixture of COOH functionalized graphene and paraffin wax.
4. Thermal stability was found out by TGA. All the samples of COOH functionalized graphene including the

paraffin wax were thermally stable. The DSC analysis also predicted that paraffin wax and paraffin wax mixed with COOH functionalized graphene have a high energy storage density along with high enthalpy of melting. The thermal conductivity and thermal diffusivity of pure paraffin wax and paraffin wax mixed with COOH graphene too showed steady increase in their values in accordance with increase in their volume% in the mixture.

Acknowledgements The authors of this paper are indebted to Lovely professional University and IIT Kanpur for providing research facilities for conduction of various characterization tests and thermal conductivity test, respectively. The authors are also thankful to Ecosense sustainable solutions private limited, New Delhi, India, for the equipment thermal energy storage system for finding energy storage, accumulated energy and energy losses including charging efficiencies.

References

1. Bhatti MM, Abdelsalam SI. Thermodynamic entropy of a magnetized Ree-Eyring particle-fluid motion with irreversibility process: a mathematical paradigm. Wiley Online Library; 2021. p. e202000186.
2. Zhang Z, Feng L, Liu H, Wang L, Wang S, Tang Z. Mo 6+P 5+ co-doped Li 2 ZnTi 3 O 8 anode for Li-storage in a wide temperature range and applications in LiNi 0.5 Mn 1.5 O 4/Li 2 ZnTi 3 O 8 full cells. Inorg Chem Front. 2022;9(1):35–43.
3. Mozaffari M, D'Orazio A, Karimipour A, Abdollahi A, Safaei MR. Lattice Boltzmann method to simulate convection heat transfer in a microchannel under heat flux: gravity and inclination angle on slip-velocity. Int J Numer Methods Heat Fluid Flow. 2019;30:3371.
4. <EcoTESTS 2.0 Product Manual - Final.pdf>.
5. Gasia J, Miró L, de Gracia A, Barreneche C, Cabeza L. Experimental evaluation of a paraffin as phase change material for thermal energy storage in laboratory equipment and in a shell-and-tube heat exchanger. Appl Sci. 2016;6(4):112. <https://doi.org/10.3390/app6040112>.
6. Nair AM, Naidu PVK. Comparison of charging and discharging period analysis of phase change materials-paraffin wax and myristic acid. Int J Curr Eng Technol. 2018. <https://doi.org/10.14741/ijcet.v8i01.10886>.
7. Kanimozhi B, Harish K, Tarun BS, Sainath Reddy PS, Sujeeth PS. Charging and discharging processes of thermal energy storage system using phase change materials. IOP Conf Ser Mater Sci Eng. 2017;197:012040. <https://doi.org/10.1088/1757-899x/197/1/012040>.
8. Wang M, Jiang C, Zhang S, Song X, Tang Y, Cheng H-M. Reversible calcium alloying enables a practical room-temperature rechargeable calcium-ion battery with a high discharge voltage. Nat Chem. 2018;10(6):667–72.
9. Zhao Q, He F, Zhang Q, Fan J, He R, Zhang K, et al. Microencapsulated phase change materials based on graphene Pickering emulsion for light-to-thermal energy conversion and management. Solar Energy Mater Solar Cells. 2019;203:110204. <https://doi.org/10.1016/j.solmat.2019.110204>.
10. Alkanhal TA. Comprehensive investigation of reduced graphene oxide (rGO) in the base fluid: thermal analysis and ANN modeling. J Ther Anal Calorim. 2021;144(6):2605–14.

11. Liu X, Rao Z. Experimental study on the thermal performance of graphene and exfoliated graphite sheet for thermal energy storage phase change material. *Thermochim Acta*. 2017;647:15–21. <https://doi.org/10.1016/j.tca.2016.11.010>.
12. Kumar P, Kumar Singh P, Nagar S, Sharma K, Saraswat M. Effect of different concentration of functionalized graphene on charging time reduction in thermal energy storage system. *Mater Today Proc*. 2021;44:146–52. <https://doi.org/10.1016/j.matpr.2020.08.548>.
13. Abd Elmaboud Y, Abdelsalam SI. DC/AC magnetohydrodynamic-micropump of a generalized Burger's fluid in an annulus. *Phys Scr*. 2019;94(11):115209.
14. Singh PK, Nagar S, Singh M. Experimental analysis of thermal efficiency of functionalized graphene (COOH) reinforced PCM for thermal energy storage system. *IOP Conf Ser Mater Sci Eng*. 2021;1116(1):012008. <https://doi.org/10.1088/1757-899x/1116/1/012008>.
15. Yang J, Jia Y, Bing N, Wang L, Xie H, Yu W. Reduced graphene oxide and zirconium carbide co-modified melamine sponge/paraffin wax composites as new form-stable phase change materials for photothermal energy conversion and storage. *Appl Therm Eng*. 2019;163:114412. <https://doi.org/10.1016/j.applthermaleng.2019.114412>.
16. Hussain A, Abidi IH, Tso CY, Chan KC, Luo Z, Chao CYH. Thermal management of lithium ion batteries using graphene coated nickel foam saturated with phase change materials. *Int J Therm Sci*. 2018;124:23–35. <https://doi.org/10.1016/j.ijthermalsci.2017.09.019>.
17. Bhatti M, Abdelsalam SI. Bio-inspired peristaltic propulsion of hybrid nanofluid flow with Tantalum (Ta) and Gold (Au) nanoparticles under magnetic effects. *Waves Random Complex Media*. 2021. <https://doi.org/10.1080/17455030.2021.1998728>.
18. Salimpour MR, Darvanjooghi MHK, Abdollahi A, Karimipour A, Goodarzi M. Providing a model for Csf according to pool boiling convection heat transfer of water/ferrous oxide nanofluid using sensitivity analysis. *Int J Numer Methods Heat Fluid Flow*. 2019;30:2867.
19. Raza R, Mabood F, Naz R, Abdelsalam SI. Thermal transport of radiative Williamson fluid over stretchable curved surface. *Therm Sci Eng Progress*. 2021;23: 100887.
20. Eldesoky I, Abdelsalam SI, El-Askary WA, Ahmed M. The integrated thermal effect in conjunction with slip conditions on peristaltically induced particle-fluid transport in a catheterized pipe. *J Porous Media*. 2020;23(7):695–713.
21. Abumandour RM, Eldesoky IM, Kamel MH, Ahmed MM, Abdelsalam SI. Peristaltic thrusting of a thermal-viscosity nanofluid through a resilient vertical pipe. *Z Naturforschung A*. 2020;75(8):727–38.
22. Elkoumy S, Barakat E, Abdelsalam S. Hall and transverse magnetic field effects on peristaltic flow of a Maxwell fluid through a porous medium. *Glob J Pure Appl Math*. 2013;9(2):187–203.
23. Peng Y, Ghahnaviyeh MB, Ahmad MN, Abdollahi A, Bagherzadeh SA, Azimy H, et al. Analysis of the effect of roughness and concentration of Fe₃O₄/water nanofluid on the boiling heat transfer using the artificial neural network: an experimental and numerical study. *Int J Therm Sci*. 2021;163:106863.
24. Longo R, Catauro M, Sorrentino A, Guadagno L. Thermal and mechanical characterization of complex electrospun systems based on polycaprolactone and gelatin. *J Therm Anal Calorim*. 2022;147:5391–9.
25. Li L, Shan Y, Wang F, Chen X, Zhao Y, Zhou D, et al. Improving fast and safe transfer of lithium ions in solid-state lithium batteries by porosity and channel structure of polymer electrolyte. *ACS Appl Mater Interfaces*. 2021;13(41):48525–35.
26. Zhang X, Tang Y, Zhang F, Lee CS. A novel aluminum–graphite dual-ion battery. *Adv Energy Mater*. 2016;6(11):1502588.
27. Bakhtiari R, Kamkari B, Afrand M, Abdollahi A. Preparation of stable TiO₂-graphene/water hybrid nanofluids and development of a new correlation for thermal conductivity. *Powder Technol*. 2021;385:466–77.

Publisher's Note Springer Nature remains neutral with regard to jurisdictional claims in published maps and institutional affiliations.